A Simplified Approach to Modelling Groundwater Dynamics in Complex, Data-Scarce Semi-Arid Basins

2. Materials and methods

2.1 Description of study area

The Noyil River sub-basin, located within the Cauvery Basin in Tamil Nadu, India, is a rapidly urbanizing region encompassing cities such as Coimbatore and Tirupur. This sub-basin features diverse land uses, including agriculture, urban, and industrial areas. Groundwater serves as a critical resource for domestic and agricultural purposes throughout the basin (Srinivasan et al., 2014; Adilakshmi et al., 2024). The semi-arid climate of the sub-basin, coupled with a history of frequent droughts, has significantly impacted groundwater availability, resulting in deeper groundwater levels in the west than in the east (Srinivasan et al., 2014). The Noyyal River was perennial till late 1970s, but it has become ephemeral river which remain dry during major part of year and flows mostly during southwest (July to September) and northeast monsoon seasons (October and November) (Sajil & James, 2016; Karunanidhi et al., 2022; Lenin et al., 2022; Krishnamoorthy et al., 2023). The basin faces challenges such as water scarcity, pollution, and degradation of natural habitats due to anthropogenic activities and climate change impact (Adilakshmi & Venkatesan, 2024). Figure 1 provides an overview of the study area, including elevation features, river networks, stream gauges, rain gauges, observation wells, and lithologs with available aquifer conductivity data. The study area is bounded by the Bhavani River to the north, the Amravati River to the south, the Cauvery River to the east, and the steeply rising Vellingiri Hills in the Western Ghats to the west, where the Noyyal river originates and flows eastward to join the Cauvery River. Elevation ranges from approximately 2,000 m in the west, gradually decreasing to 78 m in the east.

2.2 Climate and Geology of study area

The study area experiences rainfall contribution from both northeast monsoon and the southwest monsoon, with an average annual rainfall of 647 mm. The region is characterized by hot, dry conditions, with summer temperatures reaching up to 41°C, while winter temperatures drop to around 15°C (Sajil & James, 2016; Selvakumar et al., 2017). The predominant soil types include colluvial, alluvial, calcareous, non-calcareous, red, brown, and forest soils (Sajil & James, 2016; Selvakumar et al., 2017; Karunanidhi et al., 2022; Lenin et al., 2022; Sajil, 2020; CGWB, 2008). Geologically, the region is part of the peninsular gneissic complex, composed primarily of metamorphic rocks. The dominant lithologies include charnockites, granites, hornblende-biotite gneiss, sillimanite gneiss, along with basic and ultrabasic intrusives, crystalline limestone, syenite, pegmatite, and quartz veins. The major rock formations are fissile hornblende-biotite gneiss, granites, gypseous clay, and charnockite (Sajil & James, 2016; Karunanidhi et al., 2022; GSI, 1995). Aquifers in the area span from the Archaean to recent alluvium, contributing to a complex hydrogeological setting. The alluvial deposits along the Noyyal River course are key water-bearing formations, although the primary aquifers are Archaean crystalline rocks, featuring weathered fractures and joints. Groundwater storage in hard rock terrains is predominantly in fissures, fractures, and weathered zones, while porous media are more common in sedimentary formations. Gneissic formations exhibit higher degrees of weathering compared to charnockite, with weathering depths extending up to 15 meters in the granitic gneiss region and up to 8–10 meters in charnockite areas (Sajil & James, 2016; CGWB, 2008).

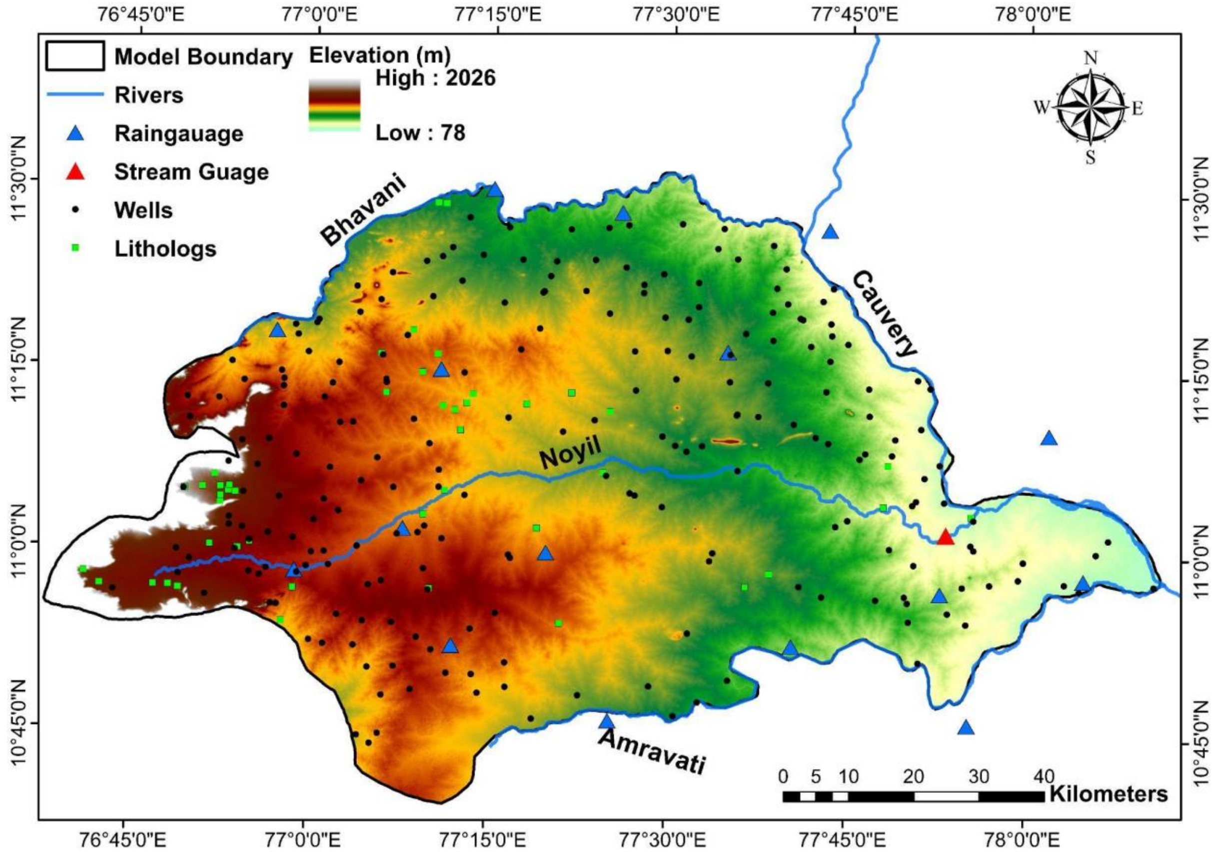

Figure -1

Overview of study area, digital elevation model and measuring instruments.

2.3 Data collection

This study utilized a combination of primary and secondary datasets from various sources to support model development and validation. Rainfall data were obtained from two key sources: (i) observational data at monthly time steps for the period 2007–2017 from 16 rain gauges managed and recorded by the Tamil Nadu (T.N.) State Department, and (ii) gridded rainfall data from the India Meteorological Department (IMD) at a spatial resolution of 0.25° and daily temporal resolution for the period 1996–2023 (Pai et al., 2015). Groundwater level observations were sourced from: (i) the T.N. State Department, which provided monthly records from 230 wells spanning 2007–2017, and (ii) the Central Ground Water Board (CGWB), recorded data which provided quarterly data for 120 wells covering the period 1996–2023. Streamflow measurements for the Noyil River were obtained from daily records maintained by the Central Water Commission (CWC). Hydraulic conductivity values were determined using results from pump tests conducted by the CGWB at 42 locations within the basin. Groundwater draft estimates were obtained from the Minor Irrigation Census survey, providing high-resolution village-level (~10 km²) data on number of wells and well distribution, categorized by well type (dug wells, shallow wells, medium wells, and deep wells). The data included average pumping hours per day during various agricultural seasons (Kharif and Rabi) and yield ranges for different well types. Secondary datasets were utilized for soft validation of modeling outputs. Actual evapotranspiration (AET) data were derived from the MODIS product (500 m spatial resolution, 8-day temporal resolution), while soil moisture data were sourced from NASA's SMAP mission. Topographic elevation details were extracted from the NASA Shuttle Radar Topography Mission (SRTM) Global 1 Arc-Second dataset (Version 003), available at a spatial resolution of 30 m.

2.4 Recharge and Draft computation

2.4.1 Initial Draft estimates

The Minor Irrigation Census data were utilized to derive initial estimates of groundwater abstraction (draft) for the basin. This dataset provided detailed information at the village level, including the number and types of wells (see Table 2.1), average daily pumping hours during various seasons (Kharif and Rabi), and yield for each well type. The assumptions on well yields are derived from the ranges provided in Minor Irrigation Census manuals and reports, crowdsourced online data, and previously published studies (see Table 2.1). Although the depths of dug wells range from 0 to over 70 meters, the majority are less than 30 meters deep, justifying the use of an assumed yield of 0.6 L/s for these wells. By utilizing the number of wells, their hourly usage, and assumed yields, a village-level (~10 km^2) map displaying pumping rates(mm/year) is generated (Fig. 4). This enabled the computation of preliminary draft estimates, which formed the basis for further model development.

2.4.2 Calculation Code

To estimate recharge and groundwater extraction in the basin, an unconfined transient groundwater model (Ambas 1D) was utilized. This model is a modified version of model adapted from Park and Parker (2008), which developed a 1-D framework specifically for unconfined aquifers. The governing equation of the model can be expressed as

$$S\frac{dh}{dt} = K\frac{d}{dx}\left(h\frac{dh}{dx}\right) \tag{1}$$

In this equation, h denotes the hydraulic head [L], t signifies time [T], S_y represents the specific yield of the aquifer system [–], and K is the hydraulic conductivity [LT^{-1}]. The authors adjusted the equation to incorporate the effects of precipitation and discharge, resulting in the following formulation (Equation 2):

$$\frac{dh}{dt} = \frac{rf}{S_y}R - \frac{1}{S_y}\lambda h \tag{2}$$

Here, λ is the discharge constant [T^{-1}], R indicates rainfall [LT^{-1}], and rf is the recharge factor [–]. The discharge constant quantifies the fraction of accessible groundwater storage that is lost laterally, reflecting groundwater loss due to local hydraulic gradients. Kumar (2012) and Subash et al. (2017) further modified this equation to account for groundwater pumping, leading to the development of the Ambhas model (CRAN - Package ambhasGW, 2017), which is a physically based model tailored for unconfined aquifers (Collins et al., 2020).

The model's governing equation is articulated as follows (Equation 3):

$$\frac{dh}{dt} = -\frac{1}{S_y}\lambda h + \frac{rf}{S_y}R - \frac{1}{S_y}D_{net} \tag{3}$$

In this equation, D_{net} represents the net groundwater abstraction [LT^{-1}], accounting for the balance between pumping and return flow. Notably, the recharge factor rf encompasses contributions from all recharge sources, including direct recharge, indirect recharge, and return flow contributions (wastewater recharge, pipe leaks etc.). The term $(1 - rf)R$ accounts for additional components of the water balance, such as evapotranspiration (ET) and runoff (Q). In this model, the recharge factor is applied directly to the total rainfall (R) rather than the effective rainfall $[R - (ET + Q)]$, thereby not considering the associated non-linear effects.

The solution to above equation can be given as follows:

$$h_{t+0.5} = h_0 + \frac{rf \cdot R - D_{\text{net}}}{S_y} \tag{4}$$

$$Discharge = S_y \cdot (1 - pd) \cdot (h_{t+0.5} - h_{\text{min}}) \tag{5}$$

$$For\ \ h_{t+0.5} \leq h_{\text{min}}\,, \quad Discharge = 0 \tag{6}$$

$$h_{t+1} = h_{t+0.5} + \frac{\text{Discharge}}{S_y} \tag{7}$$

rf is recharge factor, $p_d = 1 - \frac{1}{S_y}$ (8)

The Ambhas model has been utilized and documented in various research studies. De Bruin et al. (2012) applied it to model groundwater levels at the basin scale, while Sekhar et al. (2016) employed it to simulate groundwater dynamics in the Kabini Critical Zone Observatory. Horan et al. (2021a, 2021b) incorporated the Ambhas model to integrate groundwater routines within the Global Water Availability Assessment (GWAVA) framework. Robert et al. (2018) utilized the Ambhas model to develop a water management model at the farm level. Further, Scheidegger et al. (2021), integrated 2D lateral groundwater flow into the Variable Infiltration Capacity (VIC) model, creating the VIC-AMBHAS model. This enhanced model was subsequently used to develop a national-scale hydrological model for the Philippines. Ponnie et al. (2022) leveraged the Ambhas model to simulate daily baseflows in a tropical basin. Additionally, Shubham et al. (2022) used the model to investigate high episodic recharge events in tropical hard rock aquifers of southern India. Verma et al. 2023 utilized the model to investigate the impact of large-scale aquifer recharge using recycled water on groundwater replenishment. Recently, Baron et al. introduced the Ambhas model into the GWAVA framework to improve groundwater representation in large-scale water resource models. Jisa Joseph et al. 2022 employed the VIC-Ambhas model (Scheidegger et al., 2021) to assess the potential of transitioning from flood irrigation to drip irrigation as a strategy to mitigate groundwater depletion in the Indo-Gangetic Plains. Jisa Joseph. et. al. 2023 utilized their newly developed irrigation scheme with VIC-Ambhas model to assess impacts of irrigation on Indo-Gangetic Plains.

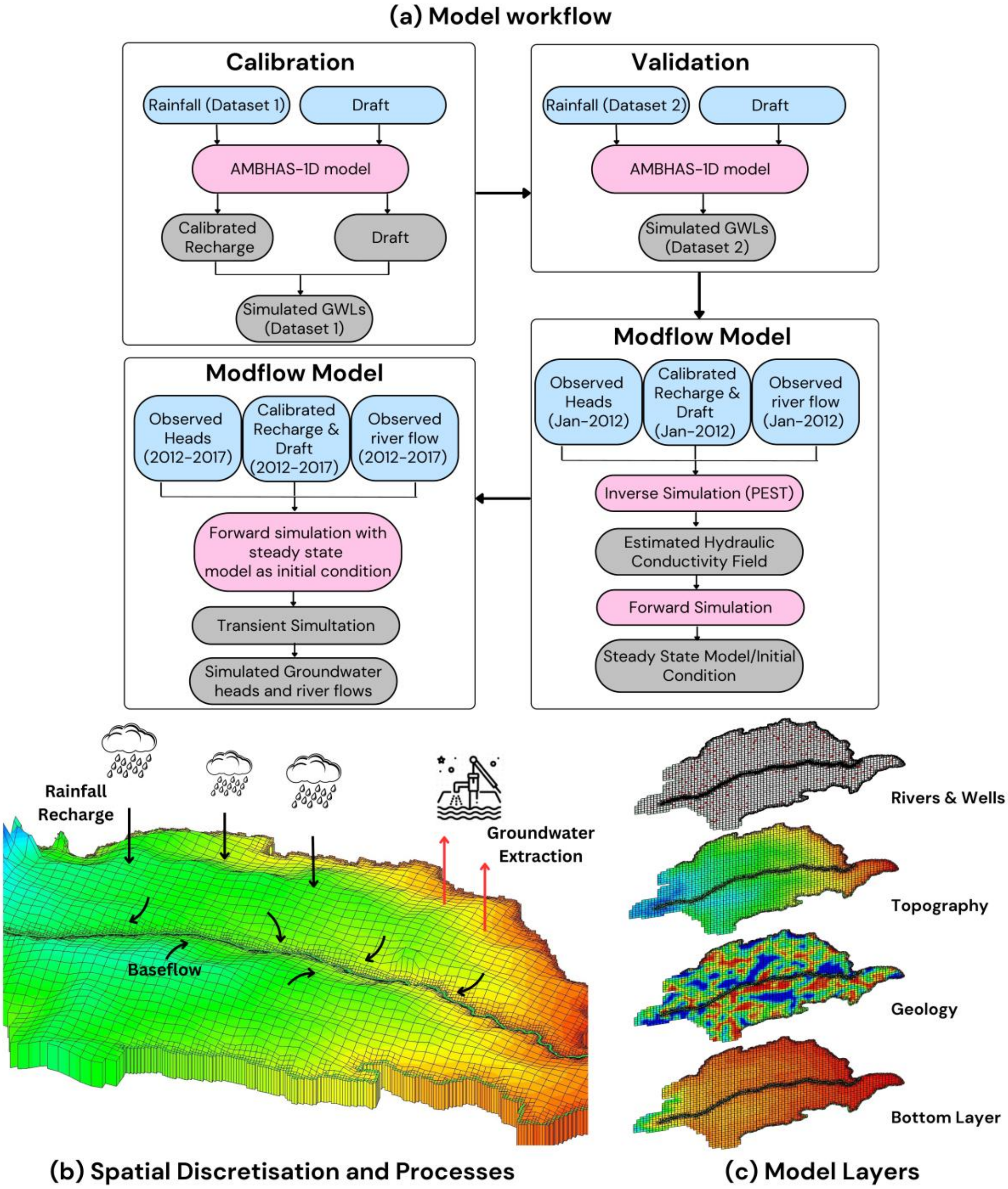

Figure 2. Schematic representation of Noyyal basin model showing **(a)** the model workflow and processes, using AMBHAS 1D model for calibration on Dataset (1) and using subsequent recharge factor from calibration to test the validation of the model on different Dataset (2) from 1996 to 2023 and then using the obtained recharge and draft as input to more complex heterogeneous numerical model to simulate groundwater depths and river flows.

Ambhas model is used with a recharge factor varying from 2% to 15% for each well. These initial guesses for the study area are taken from infiltration factors provided by CGWB reports and other basin studies. The pumping rates for the Ambhas-1D model are derived from a pumping raster (Fig. 4) and adjusted by ±10% to account for uncertainties in the estimated values. Using Dataset 1 (Table 3), the model is calibrated to produce net recharge (recharge minus pumping) for each observation well from 2007 to 2017, generating a monthly time series of calibrated distributed recharge and pumping for the basin. The calibrated recharge factors and pumping map were then applied to a long-term secondary dataset, Dataset 2 (2000–2023; Table 3), to validate the model's ability to simulate groundwater dynamics over an extended period. Given the highly anthropogenic nature of the basin, where pumping rates fluctuate significantly over time, especially during climatic stress periods, the draft was allowed to vary within a ±30% range during the validation phase to account for changes in pumping over the years.

This approach enabled the model to effectively simulate groundwater levels in observation wells while preserving the 8-11% recharge factor established during the calibration phase with Dataset 1. The variation in recharge reflects contributions from indirect sources, including surface water imports, urban pipe leaks, and wastewater infiltration, while the ±30% adjustment in pumping accommodates long-term fluctuations in groundwater abstraction. The variation in recharge will also inherently account for indirect sources of recharge, such as surface water imports, urban pipe leaks, and wastewater infiltration, while the ±30% adjustment in pumping accommodates long-term changes in groundwater abstraction. If these adjustments are not incorporated into the model, it fails to simulate long-term groundwater dynamics, indicating significant changes in groundwater use patterns over decades in the basin, as also emphasized by Srinivasan et al. (2014).

Calibration (optimx – gradient descent based optimization)

The model optimx() function from R language and optimizes the parameter to reduce the sum of squared errors in each iteration so that sum of squared errors obtained is least.

$$SSE = \sum_{i=1}^{n} \left(\mathrm{GWL}_{obs,i} - \mathrm{GWL}_{\mathrm{sim},i}\right)^2$$

Where $\mathrm{GWL}_{obs,i}$ is the observed groundwater level at time i, $\mathrm{GWL}_{\mathrm{sim},i}$ is the simulated groundwater level at time i, *and n is the number of observation values for that well.*

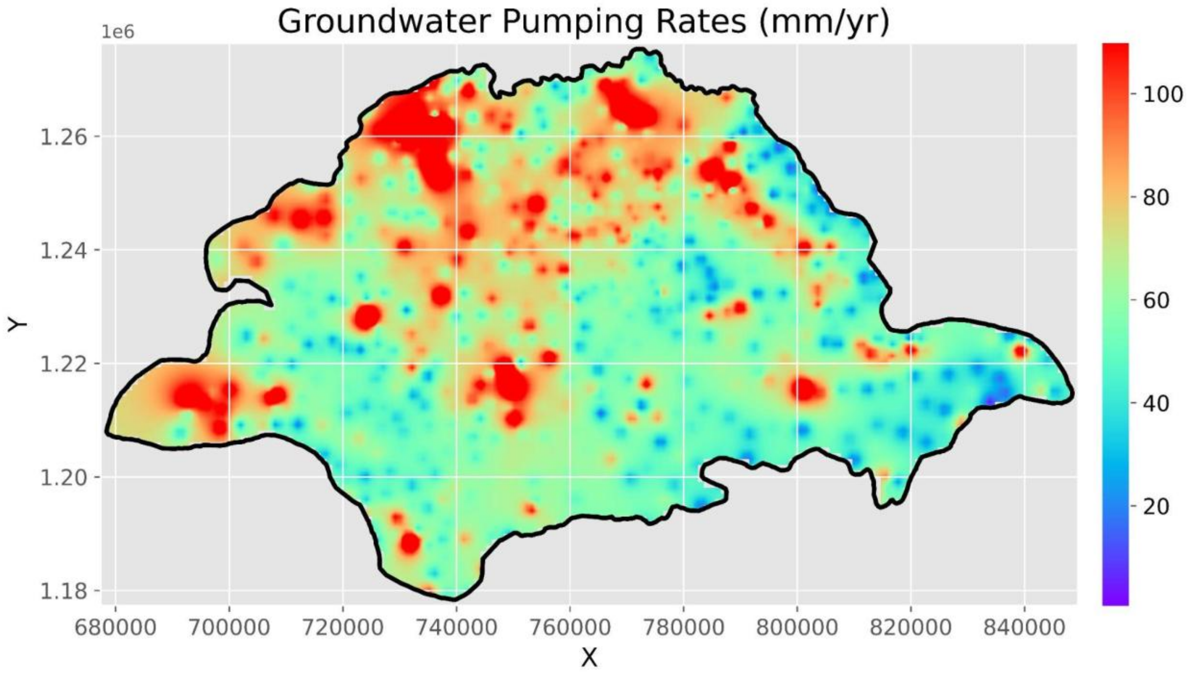

Figure 4 Groundwater abstraction map derived from minor irrigation census data, incorporating the number of different well types, their hourly pumping usage across various seasons, and the assumed yields as specified in Table 2.

Table 1. Description of various datasets used

Data Used	Source of Data	Resolution & Period	Count
Rainfall Gauge	T.N. State Department (Calibration-Dataset 1)	Monthly, (2007-2017)	16
	Indian Meteorological Department (IMD) (Validation-Dataset 2)	0.25°, Daily, (1996-2023)	12
Observation Wells	T.N. State Department (Calibration-Dataset 1)	Monthly, (2007-2017)	230
	Central Ground Water Board (Validation-Dataset 2)	Quarterly, (1996-2023)	100
Conductivity Tests	Central Ground Water Board	Noyil Basin	42
Stream Flow Gauge	Central Water commission (Validation-Numerical Model)	2000-2023	1
Irrigation Wells	Minor Irrigation Census Survey	2012-2015	1,57,365

Table 2. Description of well yield specifications for different well types.

Well Types	**Yields used**
Dugwells	0.6 L/s
Shallow Wells	0.75 L/s
Medium Wells	1L/s
Deep Wells	2 L/s

Details of datasets used for calibration and validation

Datasets	Rainfall Source	Count	Period	Observation Wells Source	Count	Period
Calibration (Dataset 1)	T.N. State Department	16	2007-2017	T.N. State Department	230	2007-2017
Validation (Dataset 2)	Indian Meteorological Department	12	1996-2023	CGWB	100	1996-2023

2.3 Numerical Simulation methods

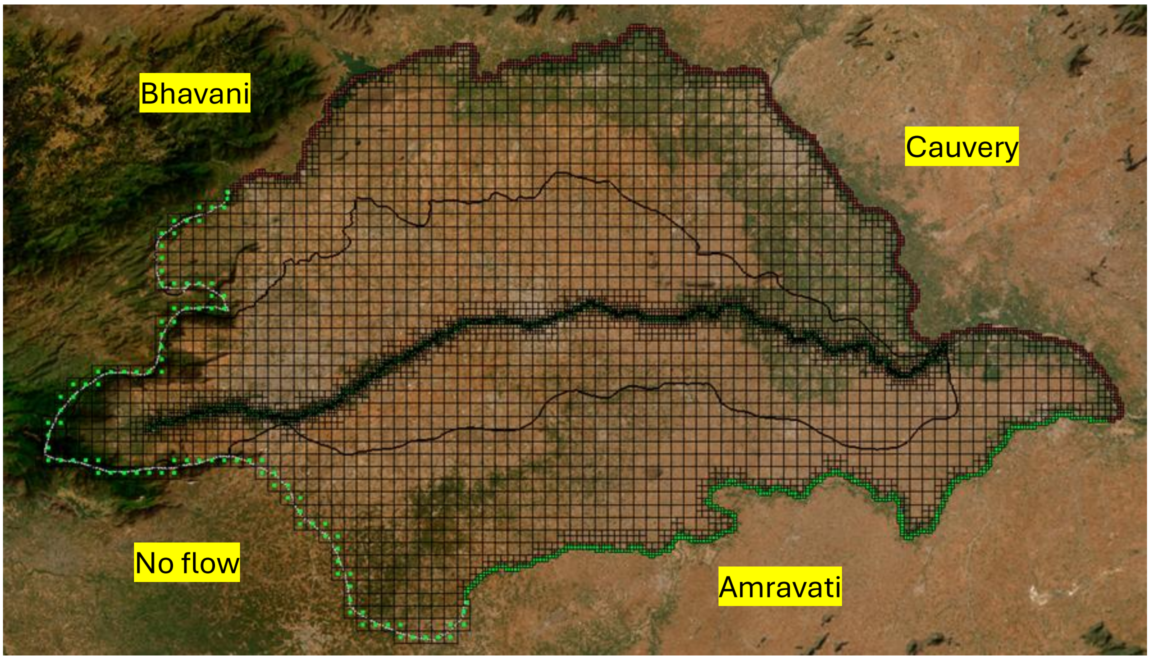

Figure 2 Numerical model with unstructured finite difference grid: 200 m grid size for the Noyil River, 500 m grid size for the river boundaries, and 2 km grid size for other areas. The boundary inside the grid is actual basin boundary achieved after stream delineation.

2.3.1 Conceptual model (e.g. BC's)

The Noyil basin covers an area of approximately 3,600 km². However, for this study, the modelled area was extended to around 8,695 km² to effectively capture the boundaries and nearby hydrological features. This extension is necessary because the sub-basin is significantly longer than it is wide, and accurate boundary representation is crucial for transient simulations because boundaries can influence the simulations. The expanded model area includes nearby rivers, which were modelled as drain and general head boundaries, an approach that best suits the study area's characteristics. Additionally, the study area is heavily influenced by human activities and contains wells deeper than 200 meters, making it unsuitable to be modelled with no-flow boundaries.

The basin was simulated and discretized using an unstructured grid mesh which is solved using the finite volume approach, implemented within the MODFLOW framework. The computational domain comprises 9,978 cells with variable spatial resolutions, tailored to capture the distinct geographical and topographical features of the basin. The Noyil River was modelled with a fine grid size of 200 meters, where it was conceptualized as a drain boundary to reflect its geomorphology and hydrological dynamics precisely.

The model domain is bounded by the Bhavani River to the north, the Amravati River to the south, the Cauvery River to the east, and a mountainous region to the west. The Bhavani and Cauvery rivers were represented as general head boundaries (GHB), while the Amravati River was treated as a drain boundary. The grid discretization was primarily 2 km by 2 km across the region, with exceptions: the Noyil River was modeled using a finer grid of 200 meters, and the boundary areas to the east, west, north, and south were modeled at a 500-meter resolution.

The basin's elevation data were derived from the NASA Shuttle Radar Mission Global 1 arc-second V003 dataset, with elevation values assigned to the top of each grid cell. The conceptual model's base, representing bedrock, was set at a depth of 100 meters below the surface. Hydraulic conductivity values, obtained from field pump tests, were incorporated into the model, with specific locations and dataset details provided in Fig. 1 and Table 1.

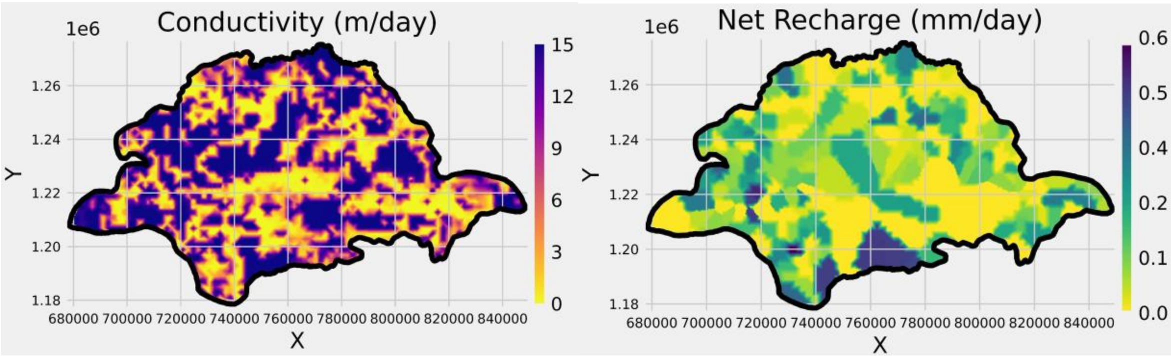

Figure 3

Conductivity field generated from inverse PEST simulation and recharge field fed to the steady state simulation.

2.3.2 Initial condition

The study area is characterized by data scarcity and discontinuous records, particularly lacking borehole transmissivity data across the region. To address this, inverse modeling was conducted using PEST to generate conductivity field for the study area. Pilot points were assigned to grid cells, each initialized with an estimated hydraulic conductivity based on regional studies and provided with a specified range for adjustment. Grid cells where pump test conductivity values were available were treated as fixed pilot points, meaning that the conductivity at those locations remained constant during the inverse simulation process. This approach effectively incorporated the actual pump test results into the model, preserving the observed field data while optimizing the conductivity for other areas.

The model was supplied with net recharge estimates for January 2012, obtained from the AMBHAS_1D model. PEST then iteratively adjusted the hydraulic conductivity values at the pilot points to minimize the discrepancies between the simulated and observed groundwater heads at observation wells, as well as the simulated baseflow for the dry period in January 2012. The algorithm repeatedly executed forward model runs, each time refining the parameter values to progressively reduce the error.

The inverse simulation ran for approximately 14 hours on a 12th Gen Intel(R) Core (TM) i9-12900K processor (64gb RAM), utilizing all available cores and parallel computation capabilities. The process continued until the error in groundwater head simulation and baseflow was reduced to acceptable limits. Figures 3(a) and 3(b) show the resulting conductivity field from the inverse simulation and the net recharge input used in the process. Using the conductivity field generated, we conducted a forward model run to get a calibrated steady state model which establishes the initial conditions for subsequent transient numerical simulations.

2.3.3 Transient simulation

The steady-state head distribution from January 2012 is used as the initial condition for our model. The time series of net recharge, derived from the 1-D model, serves as input for the dynamic model, which operates on monthly time steps. This methodology allows for the detailed analysis of groundwater dynamics, river base flows during dry periods, and the simulation of groundwater well hydrographs.

The period from 2012 to 2017 was selected for the numerical simulation due to the availability of monthly time step data for this interval. Additionally, the objective of this study is to present a methodology for modelling a sparsely monitored, climate-impacted semi-arid basin with substantial anthropogenic influences.

4. Results and Discussions

The term $(1 - rf)R$ in the model represents additional components of the water balance, including evapotranspiration (ET) and runoff (Q). Unlike approaches that consider effective rainfall [$R - (ET + Q)$], this model applies the recharge factor directly to total rainfall (R), thereby simplifying the calculation by avoiding the inclusion of non-linear interactions between components. The basin's mixed land use, comprising agricultural, urban, and industrial sectors, introduces complexity to groundwater recharge processes. Factors such as surface water imports, pipeline leakages, and wastewater recharge contribute to the recharge dynamics, making it challenging to isolate individual contributions. By incorporating these factors collectively, the recharge factor effectively represents the overall recharge scenario in the basin without disaggregating individual components. This integrated approach makes the model particularly well-suited for basins with diverse and overlapping land-use patterns.

Figure 5 displays a comparison between observed mean heads and calibrated simulated heads based on Dataset 1, which includes rainfall and groundwater observations from the T.N. State Department. The 1-D model was initially calibrated using finely calculated pumping rates with a ±20% variation and recharge rates ranging from 2% to 16%. The calibrated model estimated the rainfall recharge to be approximately 9.67%. To validate this calibration, the model was applied to an entirely different long-term dataset, Dataset 2, which consists of rainfall data from the IMD and groundwater observations from the CGWB, covering the period from 1996 to 2023.

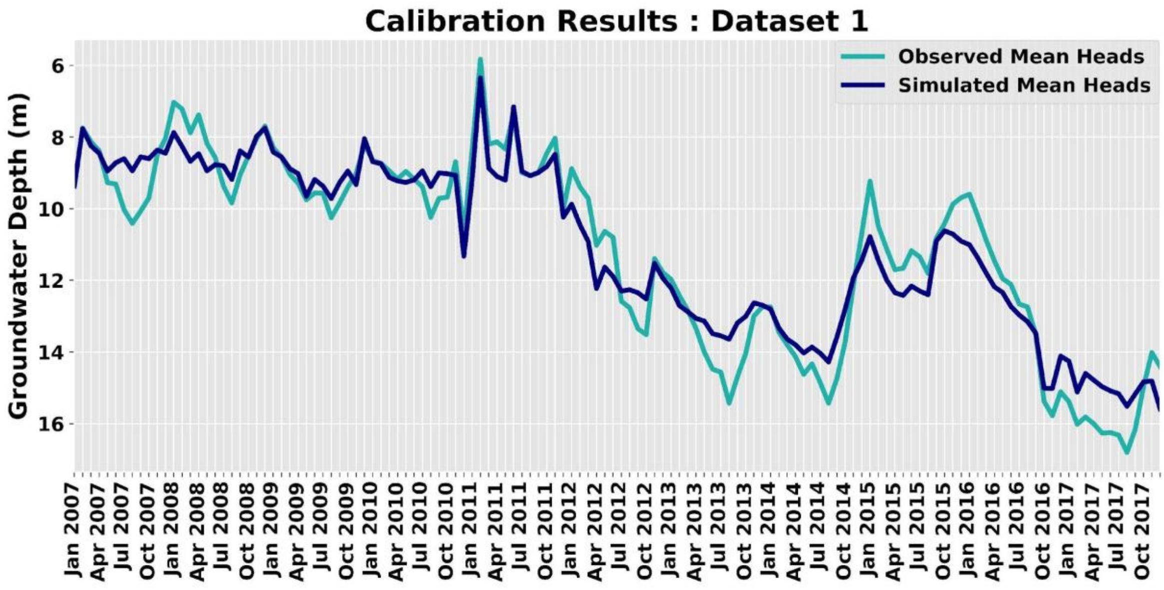

Figure 5

Hydraulic heads derived from the calibrated Ambhas-1D model using Dataset 1 (source: State Department Wells and Rain Gauges)

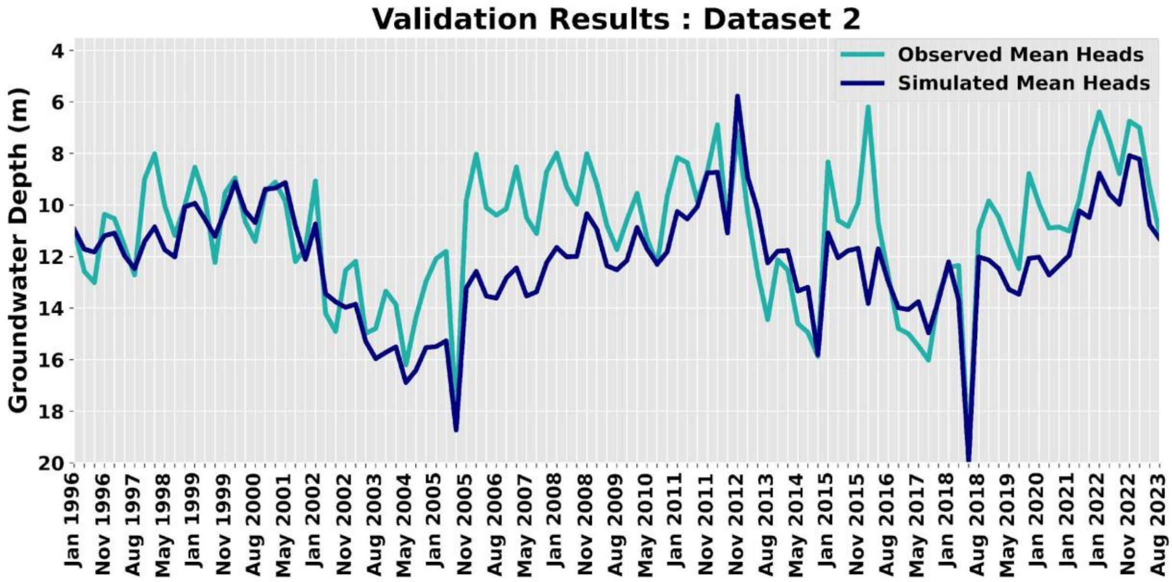

Figure 6

Validation results based on Dataset 2 (sources: rainfall data from IMD and well data from CGWB)

Figure 6 presents a comparison between observed and simulated long-term groundwater heads from the validation model, using a recharge rate of 9.67% and calibrated pumping rates. The model successfully simulates the long-term groundwater head trends in the basin; however, it does not effectively capture the peaks observed around 2005 and 2015. This discrepancy could be attributed to several factors, such as the application of the validation model to an entirely different dataset, as well as the model's inability to accurately represent sharp groundwater fluctuations that occur over short periods due to heavy rainfall events. Validation on Dataset 2 was performed to determine whether the model-generated outputs—specifically, the time series of net recharge (recharge minus pumping)—are suitable for use in the subsequent numerical MODFLOW model. The validation results demonstrate the model's capability to capture groundwater dynamics over extended periods. This finding enables us to generate inputs for a more complex transient numerical model operating on monthly time steps.

The numerical model is initialized using the calibrated net recharge for January 2012 and the estimated hydraulic conductivity field to perform a forward simulation. Figure 6 presents a scatter plot comparing simulated and observed heads for January 2012 across 208 observation wells, yielding an R-squared of 0.998 and an RMSE of 3.542 meters. The forward simulation also estimated river flow with an error margin of less than 2.6% (Table 2). These results suggest that the simulated groundwater heads from the forward run can serve as initial conditions for the subsequent transient model. Figures 7(a) and 7(b) display maps of the estimated groundwater depths and heads, respectively.

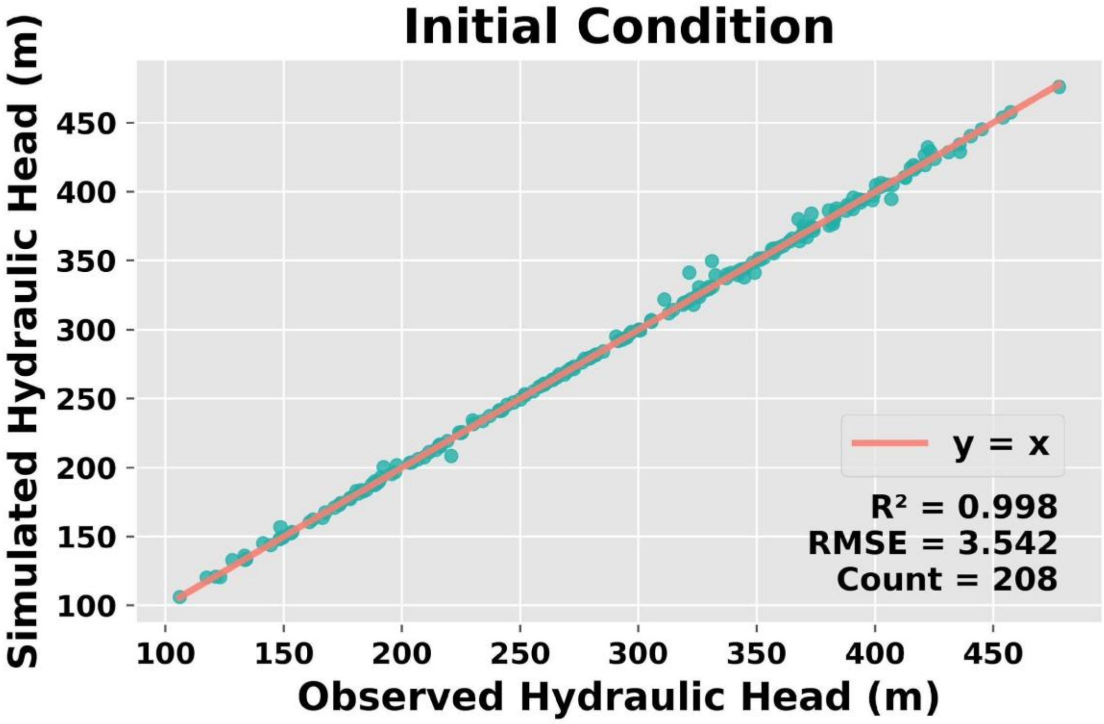

Figure 7

Comparison of simulated and observed hydraulic heads from the steady-state numerical simulation (Initial condition)

Baseflow

Observed Baseflow in 2012 (m^3/d)	**Computed Baseflow (m^3/d)**	**Residual**	**Error (%)**
200327.0	205521.3	5194.3	<2.6%

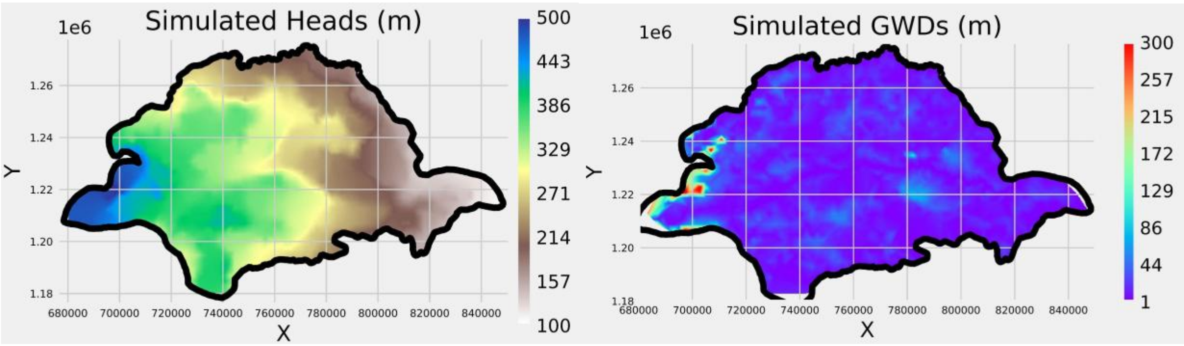

Figure 8

Simulated hydraulic heads and groundwater depths (GWDs) utilized as initial conditions for the transient numerical model.

A transient numerical simulation was conducted using inputs derived from the 1-D model, with monthly time steps covering the period from 2012 to 2017, to analyse groundwater dynamics within the basin. Figure 8 presents a scatter plot comparing simulated and observed heads, based on 11,063 observation points, with an R-squared value of 0.997 and an RMSE of 4.5 meters. It is important to note that the transient numerical model was not calibrated; it directly utilized the time series inputs from the 1-D model. Figure 9 shows the observed and simulated river flows during dry periods for the simulation period. The transient model effectively captures river flows during dry periods, except for April and May in the years 2015 and 2016. This discrepancy may be attributed to unanticipated releases from the non-operational upstream Orathupalayam Dam, which was primarily used for irrigation. Unfortunately, data on water releases from this small dam is not available.

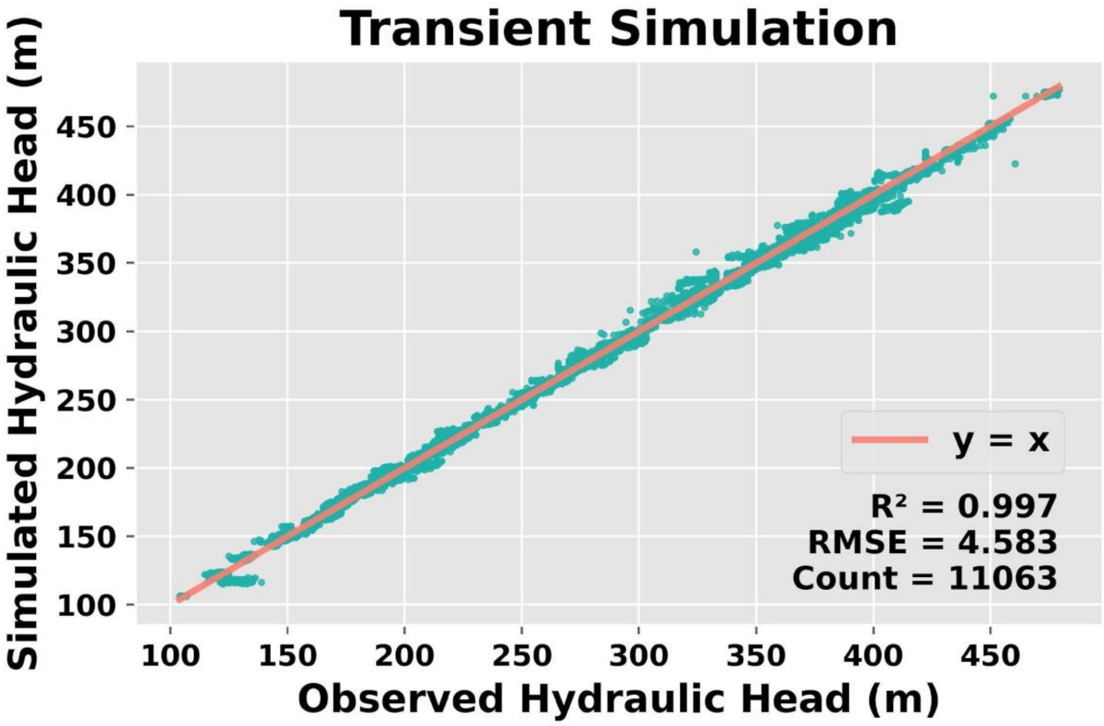

Figure 9

Scatter plots comparing simulated and observed monthly groundwater heads for the period 2012-2017, derived from the monthly time-step transient numerical model.

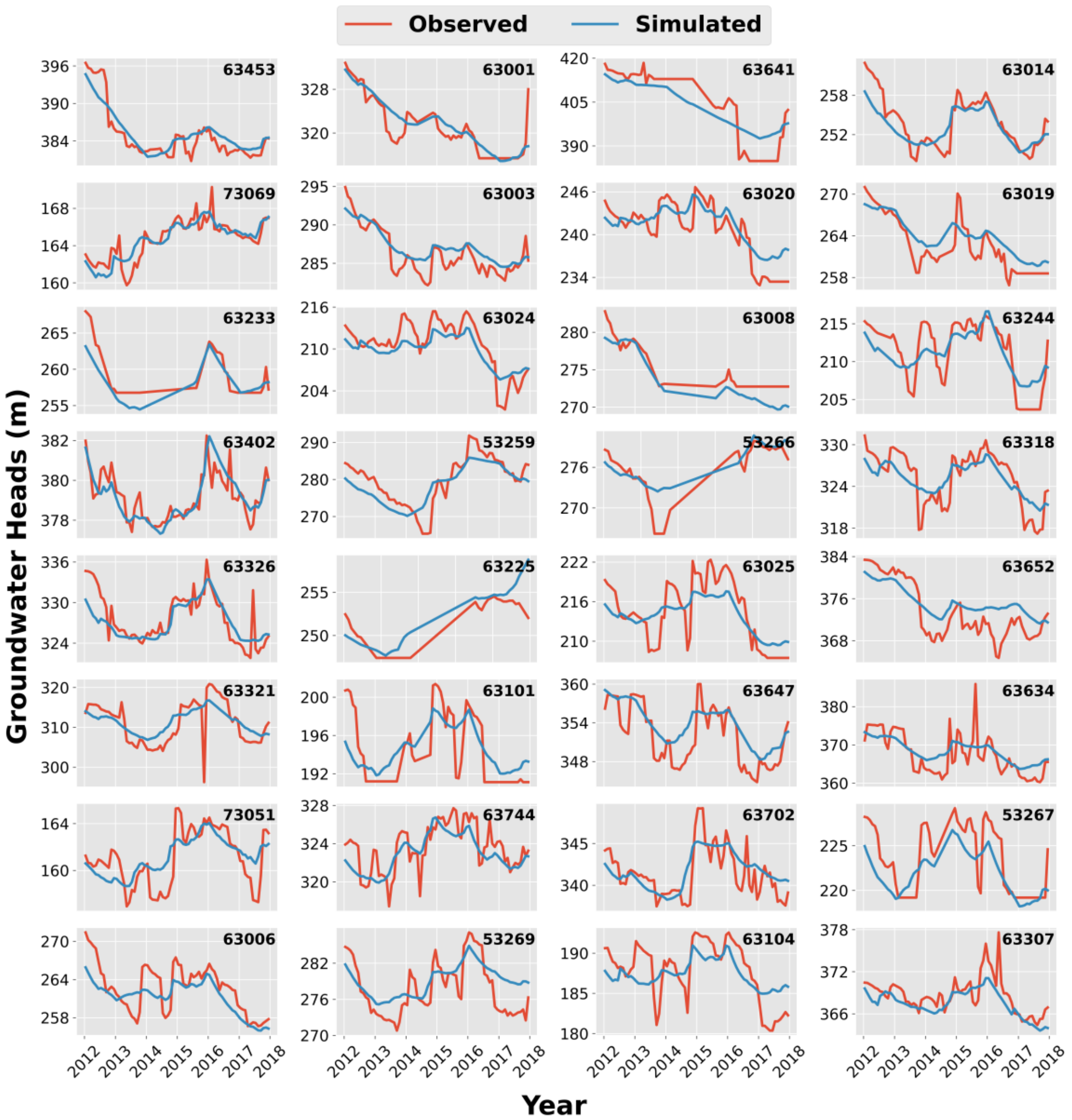

Figure 10

Plots of observed versus simulated groundwater heads on a monthly timescale from January 2012 to December 2017, with well numbers indicated in each subplot. Note that not all wells are displayed here; additional plots for other wells are provided in the supplementary material.

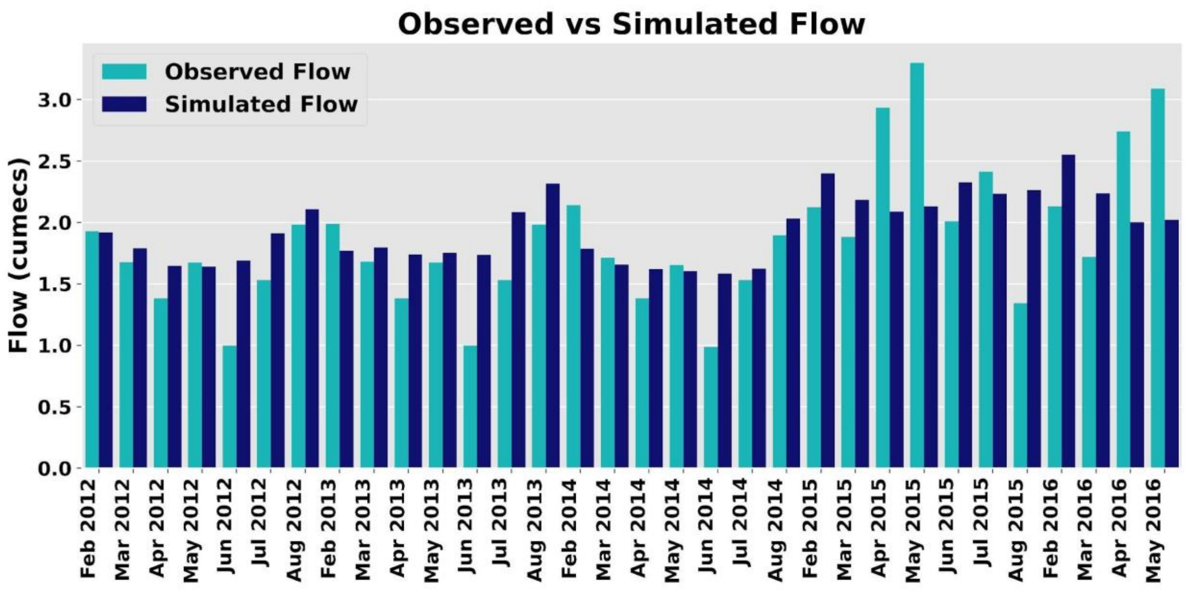

Figure 10

Measured monthly dry-period flow rates versus simulated flow rates from the transient numerical model.

Figure 10 illustrates groundwater dynamics captured by the numerical models in comparison to observed data, showing changes in net and cumulative storage within the basin at each time step. It also depicts the variations in base flow corresponding to each monthly time step, highlighting the advantage of using numerical models. The figure indicates that as groundwater depths become shallower, the contribution of base flow to the river increases due to a greater volume of water available in aquifer storage to sustain river flow. From January 2012 to July 2014, as groundwater depth declines, there is a predominantly positive net storage loss, indicating that the aquifer is losing storage mainly due to over-abstraction during the drought years of 2013 and 2014, when pumping exceeded recharge. Cumulative storage change also shows a continuous increase during this period, reflecting the total volume of water lost from aquifer storage. In late 2014 and early 2015, heavy rainfall events contributed to significant recharge of the aquifer, leading to positive net storage gain and a decrease in total cumulative storage loss. These results demonstrate the variability in aquifer storage changes at each time step, governed by the complex interactions between recharge and pumping. Overall, from 2012 to 2017, the aquifer experienced a net storage loss, with groundwater depths declining from 8 to 14 meters

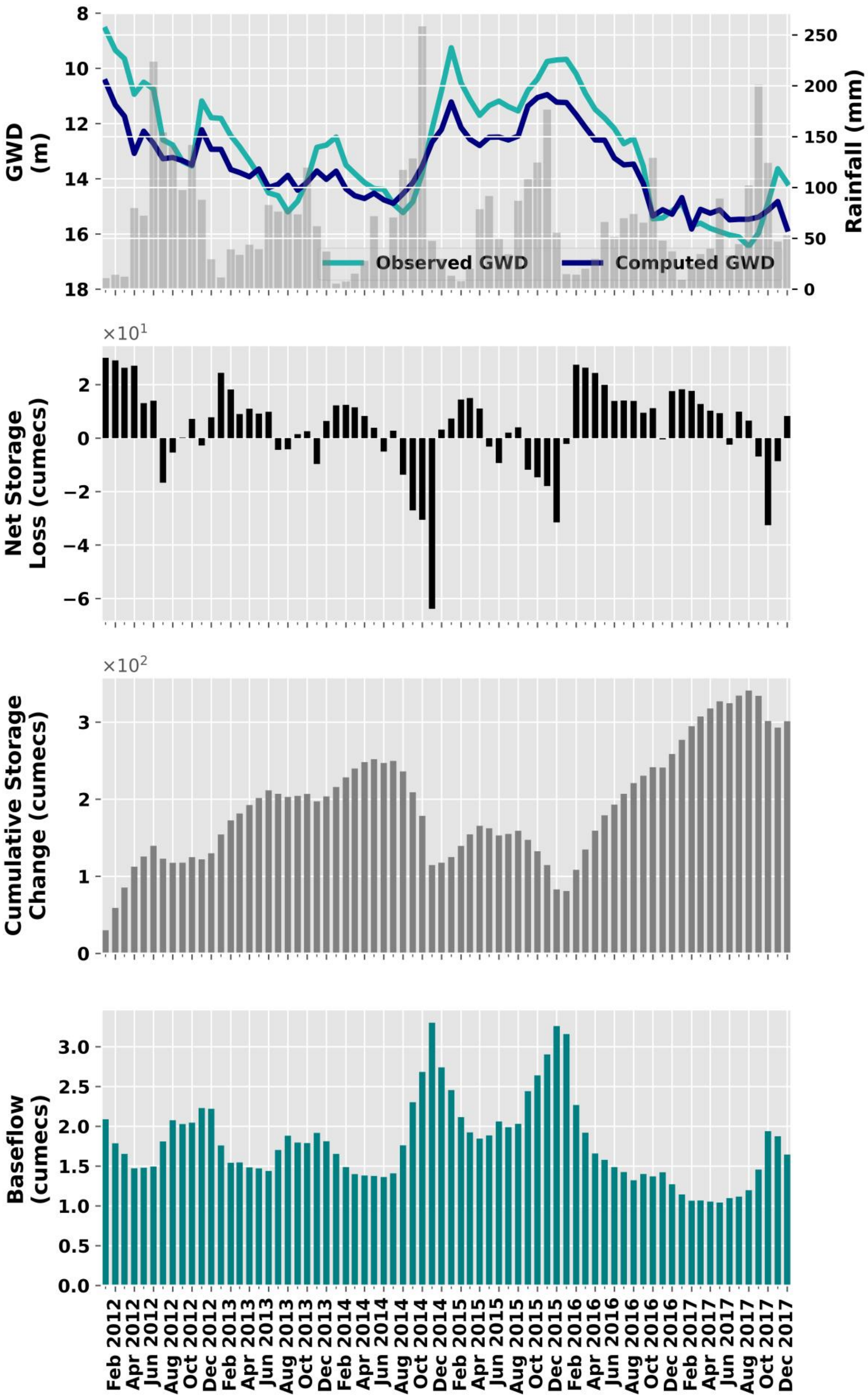

GWD (m)
Rainfall (mm)
Observed GWD
Computed GWD
Net Storage Loss (cumecs)
×10^1
Cumulative Storage Change (cumecs)
×10^2
Baseflow (cumecs)
Feb 2012
Apr 2012
Jun 2012
Aug 2012
Oct 2012
Dec 2012
Feb 2013
Apr 2013
Jun 2013
Aug 2013
Oct 2013
Dec 2013
Feb 2014
Apr 2014
Jun 2014
Aug 2014
Oct 2014
Dec 2014
Feb 2015
Apr 2015
Jun 2015
Aug 2015
Oct 2015
Dec 2015
Feb 2016
Apr 2016
Jun 2016
Aug 2016
Oct 2016
Dec 2016
Feb 2017
Apr 2017
Jun 2017
Aug 2017
Oct 2017
Dec 2017

Figure 11

Mean observed GWD depth versus simulated GWD, Storage changes and baseflow as computed by the dynamic model

5. Conclusion

Semi-arid basins, characterized by climate extremes such as prolonged rainfall deficits, often experience heightened dependence on groundwater resources due to limited surface water availability. In basins dominated by anthropogenic activities, this reliance exacerbates water stress during rainfall deficit periods, potentially leading to drought conditions. Understanding groundwater dynamics in such basins poses significant challenges, particularly in data-scarce regions where critical information on recharge and groundwater abstraction (pumping) is often insufficient to develop robust dynamic groundwater models. Additionally, accurately quantifying recharge and abstraction across diverse land-use types adds another layer of complexity, further complicating effective groundwater management and modeling efforts.

A water table fluctuation method based 1-D model was utilized to estimate the recharge and pumping characteristics of the basin. The model was calibrated using Dataset 1 and validated against a completely independent data source, Dataset 2, to assess its effectiveness. The study highlights the necessity of incorporating finer-scale attributes, such as anthropogenic water use, which are frequently disregarded due to data scarcity. The study illustrates how calibrated time series outputs from a straightforward water table fluctuation-based 1-D model can serve as inputs for a more complex, physically based transient numerical model. Transient numerical model was applied without any calibration, relying solely on the time series inputs generated by the 1-D model. This approach is particularly well-suited for data-limited, semi-arid regions with unpredictable rainfall and substantial anthropogenic water use, presenting considerable challenges for water security during drought periods when groundwater is the primary water source. The model allows for the detailed analysis of groundwater dynamics, flow behaviour during dry periods, and the effective management of water resources in water-stressed basins.

Validation model using Dataset 2 showed increase in groundwater draft similar to observations made by Srinivasan et. al. The rainfall recharge is applied directly after calibrating the system, this recharge factor considers all kinds or recharge (direct, indirect) without their separation, and thus this kind of approach of modelling a system can be suitable for highly complex mixed basins with limited data available. Using soft validation results show that even in periods of low rainfall GW use for irrigation does not stop – this causes the depletion of Groundwater levels in the basin. Which later refills or recharges after sufficient rain. This means the Groundwater in such basins are directly tied to rainfall recharge.

6. References

Ponni Mariet George, M Sekhar, Base flow simulation using a physically based subsurface model – The case of a tropical basin in the Western Ghats, India, Journal of Hydrology, Volume 613, Part B, 2022, 128451, ISSN 0022-1694, https://doi.org/10.1016/j.jhydrol.2022.128451.

Eungyu Park, J.C. Parker, A simple model for water table fluctuations in response to precipitation, Journal of Hydrology, Volume 356, Issues 3–4, 2008.

Subash, Y., Sekhar, M., Tomer, S.K., Sharma, A.K., 2017. A framework for assessment of climate change impacts on the groundwater system. In: Ojha, C.S.P., Rao, S., Zhang, T., Bardossy, A. (Eds.), Sustainable Water Resources Management, Vol. 14. ASCE.

D. Karunanidhi, P. Aravinthasamy, T. Subramani, Rohana Chandrajith, N. Janardhana Raju, I.M.H.R. Antunes, Provincial and seasonal influences on heavy metals in the Noyyal River of South India and their human health hazards, Environmental Research,Volume 204, Part A, 2022,111998, ISSN 0013-9351, https://doi.org/10.1016/j.envres.2021.111998.

GSI, 1995. Geological and Mineral Map of Tamil Nadu and Pondicherry. Published by the Director General Geological Survey of India on 1: 500,000 scale.

M. Lenin Sundar, S. Ragunath, J. Hemalatha, S. Vivek, M. Mohanraj, V. Sampathkumar, A. Mohammed Siraj Ansari, V. Parthiban, S. Manoj, Simulation of ground water quality for noyyal river basin of Coimbatore city, Tamilnadu using MODFLOW, Chemosphere, Volume 306, 2022, 135649, ISSN 0045-6535, https://doi.org/10.1016/j.chemosphere.2022.135649.

N. Krishnamoorthy, R. Thirumalai, M. Lenin Sundar, M. Anusuya, P. Manoj Kumar, E. Hemalatha, M. Mohan Prasad, Neha Munjal, Assessment of underground water quality and water quality index across the Noyyal River basin of Tirupur District in South India, Urban Climate, Volume 49, 2023, 101436, ISSN 2212-0955,https://doi.org/10.1016/j.uclim.2023.101436.

P.J. Sajil Kumar & E.J. James (2016) Identification of hydrogeochemical processes in the Coimbatore district, Tamil Nadu, India, Hydrological Sciences Journal, 61:4, 719-731, DOI: 10.1080/02626667.2015.1022551

S. Selvakumar, N. Chandrasekar, G. Kumar, Hydrogeochemical characteristics and groundwater contamination in the rapid urban development areas of Coimbatore, India, Water Resources and Industry, Volume 17, 2017, Pages 26-33, ISSN 2212-3717, https://doi.org/10.1016/j.wri.2017.02.002.

Adilakshmi A, Venkatesan V, Effective monitoring of Noyyal River surface water quality using remote sensing and machine learning and GIS techniques, Desalination and Water Treatment, Volume 320, 2024, 100630, ISSN 1944-3986, https://doi.org/10.1016/j.dwt.2024.100630.

Pranesh Kumar Paul, Selecting hydrological models for developing countries: Perspective of global, continental, and country scale models over catchment scale models, https://doi.org/10.1016/j.jhydrol.2021.126561

Pai, D. S., Sridhar, L., Badwaik, M. R., & Rajeevan, M. (2015). Analysis of the daily rainfall events over India using a new long period (1901–2010) high resolution (0.25° × 0.25°) gridded rainfall data set. Climate Dynamics, 45(3–4), 755–776. https://doi.org/10.1007/ s00382-014-2307-1

[Rebecca, Review: Current and emerging methods for catchment-scale modelling of recharge and evapotranspiration from shallow groundwater. DOI 10.1007/s10040-016-1470-3

Esra, A pre-calibration approach to select optimum inputs for hydrological models in data-scarce regions, doi:10.5194/hess-20-4391-2016

E. M. de Graaf, A high-resolution global-scale groundwater model, doi:10.5194/hess-19-823-2015

Condon, L. E., and R. M. Maxwell (2015), Evaluating the relationship between topography and groundwater using outputs from a continental-scale integrated hydrology model, Water Resour. Res., 51, 6602– 6621, doi:10.1002/2014WR016774

Hellwig, J., de Graaf, I. E. M., Weiler, M., & Stahl, K. (2020). Large-scale assessment of delayed groundwater responses to drought. Water Resources Research, 56, e2019WR025441. https:// doi.org/10.1029/2019WR025441

Nie, W., Zaitchik, B. F., Rodell, M., Kumar, S. V., Anderson, M. C., & Hain, C. (2018). Groundwater withdrawals under drought: Reconciling GRACE and Land Surface Models in the United States High Plains Aquifer. Water Resources Research, 54, 5282–5299. https://doi. org/10.1029/2017WR022178

Kumar, R., Musuuza, J. L., Van Loon, A. F., Teuling, A. J., Barthel, R., Ten Broek, J., et al. (2016). Multiscale evaluation of the Standardized Precipitation Index as a groundwater drought indicator. Hydrology and Earth System Sciences, 20(3), 1117–1131. https://doi.org/10.5194/ hess-20-1117-2016

Van Loon, A. F., Gleeson, T., Clark, J., van Dijk, A. I. J. M., Stahl, K., Hannaford, J., Di Baldassarre, G., Teuling, A. J., Tallaksen, L. M., Uijlenhoet, R., Hannah, D. M., Sheffield, J., Svoboda, M., Verbeiren, B., Wagener, T., Rangecroft, S., Wanders, N., and Van Lanen, H. A. J.: Drought in the Anthropocene, Nat. Geosci., 9, 89–91, 2016

Heudorfer, B., Haaf, E., Stahl, K., & Barthel, R. (2019). Index-based characterization and quantification of groundwater dynamics. Water Resources Research, 55, 5575–5592. https://doi.org/10.1029/2018WR024418

Cgwb, District Groundwater Brochure Coimbatore District, Tamil Nadu.

CGWB Technical Report Series, 2008.

Sajil Kumar, P. J. (2020). Fluoride enrichment in groundwater and associated human health risk in a tropical hard rock terrain in South India. Human and Ecological Risk Assessment: An International Journal, 27(4), 1037–1053. https://doi.org/10.1080/10807039.2020.1799185

Marion Robert, Alban Thomas, Muddu Sekhar, Shrinivas Badiger, Laurent Ruiz, Hélène Raynal, Jacques-Eric Bergez,

Adaptive and dynamic decision-making processes: A conceptual model of production systems on Indian farms, Agricultural Systems, Volume 157, 2017, Pages 279-291, ISSN 0308-521X, https://doi.org/10.1016/j.agsy.2016.08.001.

Horan, R.; Rickards, N.J.; Kaelin, A.; Baron, H.E.; Thomas, T.; Keller, V.D.J.; Mishra, P.K.; Nema, M.K.; Muddu, S.; Garg, K.K.; et al. Extending a Large-Scale Model to Better Represent Water Resources without Increasing the Model's Complexity. Water 2021, 13, 3067. https://doi.org/10.3390/w132130

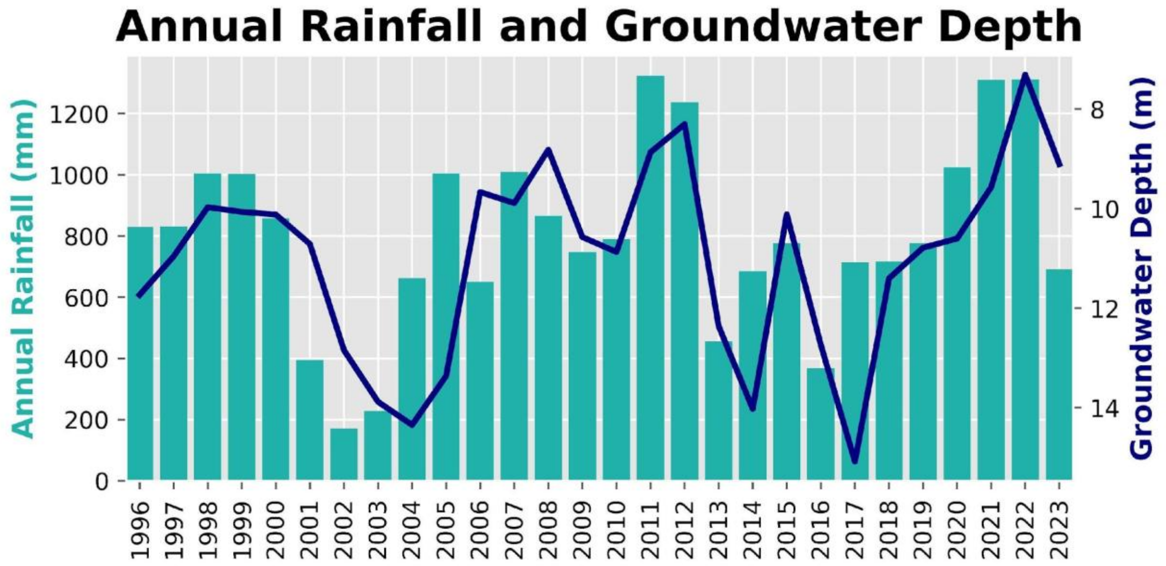

Figure 12

Long term annual rainfall versus mean observed groundwater depth in the basin.

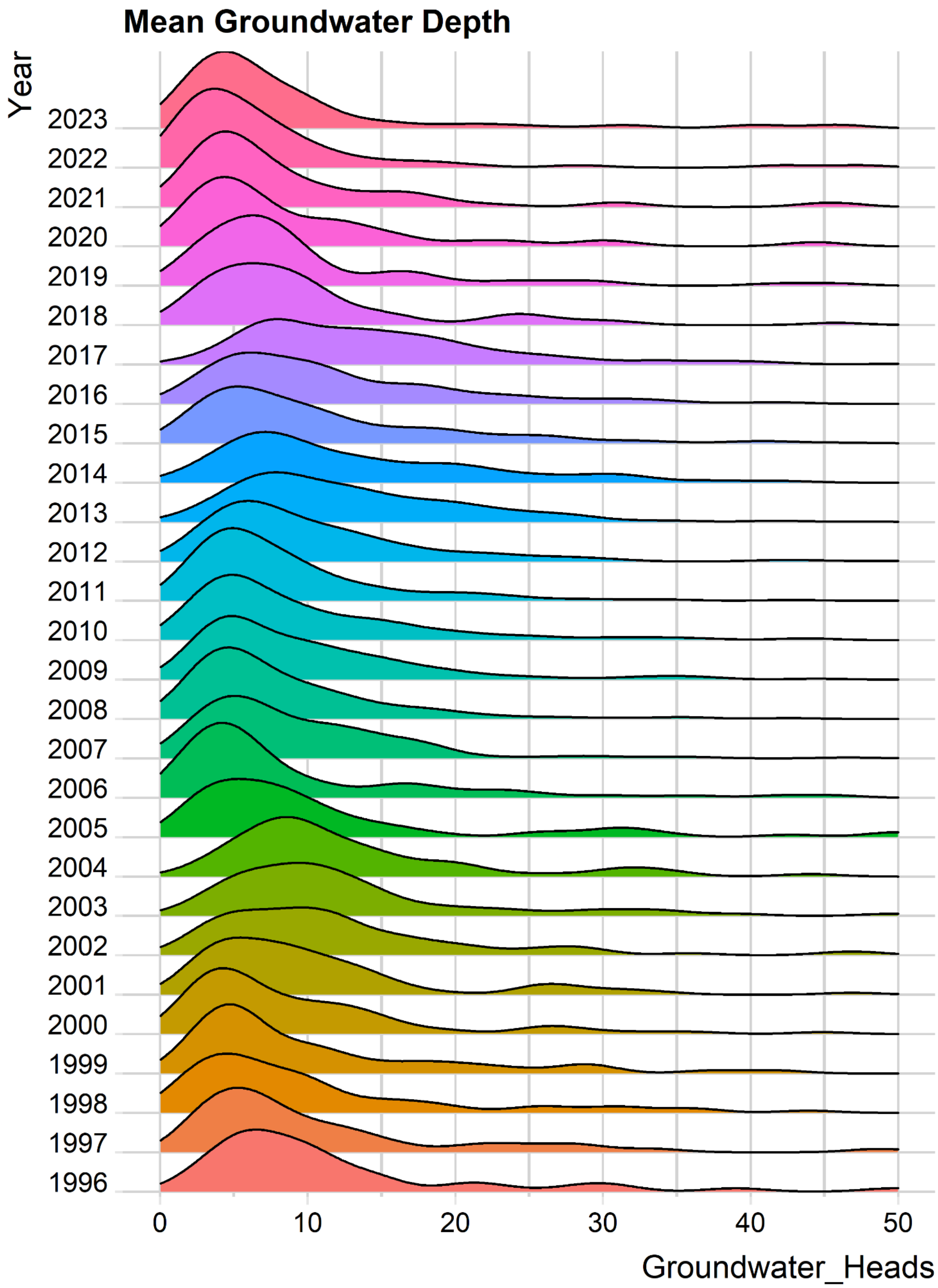
Mean Groundwater Depth
Year
2023
2022
2021
2020
2019
2018
2017
2016
2015
2014
2013
2012
2011
2010
2009
2008
2007
2006
2005
2004
2003
2002
2001
2000
1999
1998
1997
1996
0
10
20
30
40
50
Groundwater_Heads

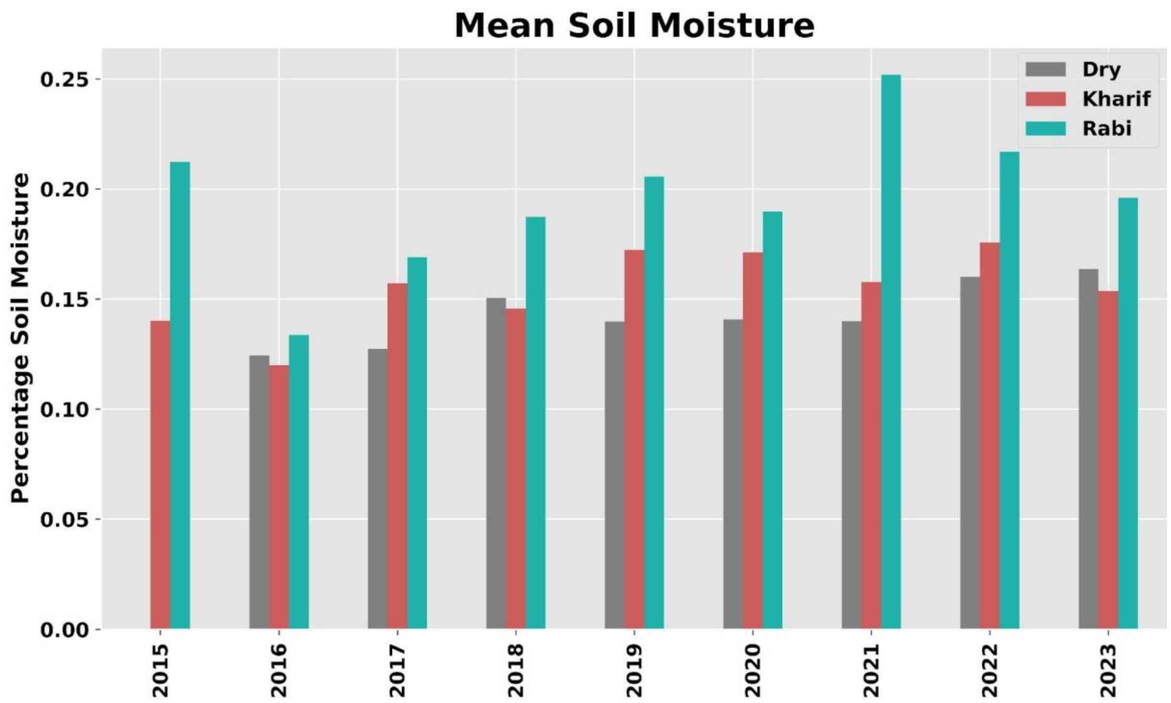

Figure 13

Mean soil moisture over the basin during different periods over the years.

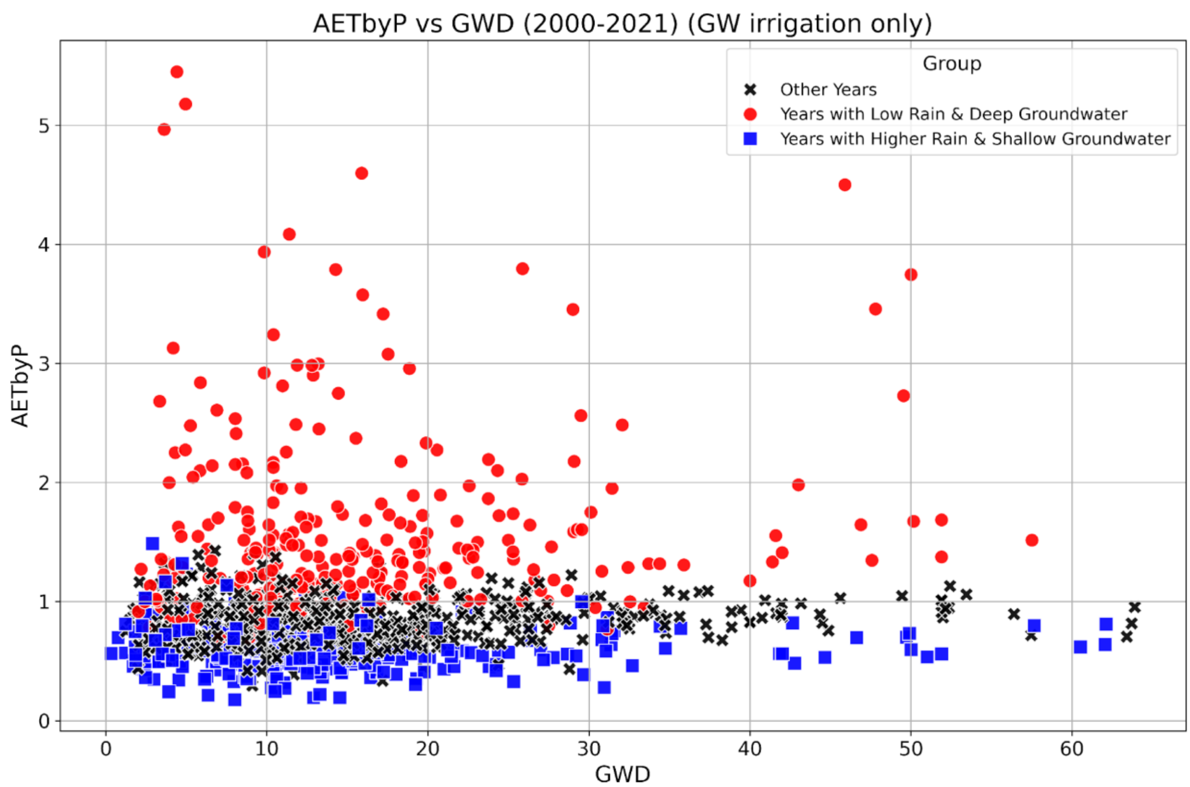

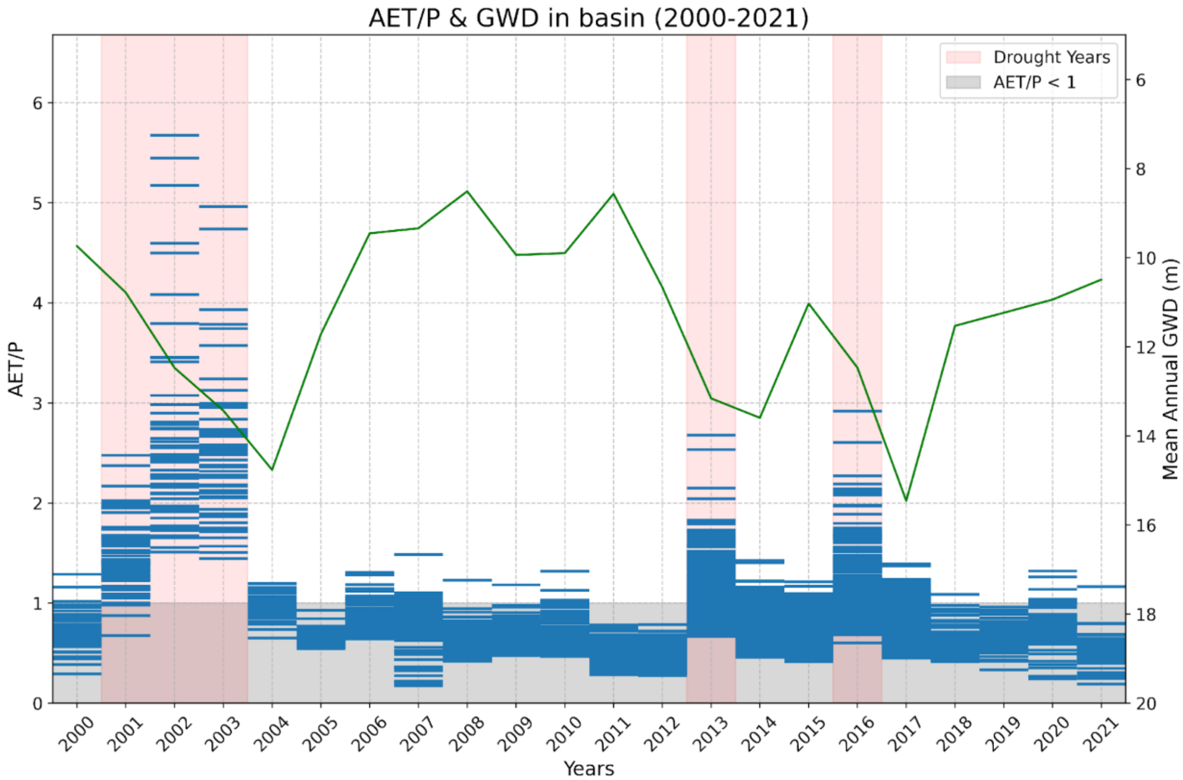

AET/P & GWD in basin (2000-2021)
Drought Years
AET/P < 1
AET/P
Mean Annual GWD (m)
Years
0
1
2
3
4
5
6
6
8
10
12
14
16
18
20
2000
2001
2002
2003
2004
2005
2006
2007
2008
2009
2010
2011
2012
2013
2014
2015
2016
2017
2018
2019
2020
2021

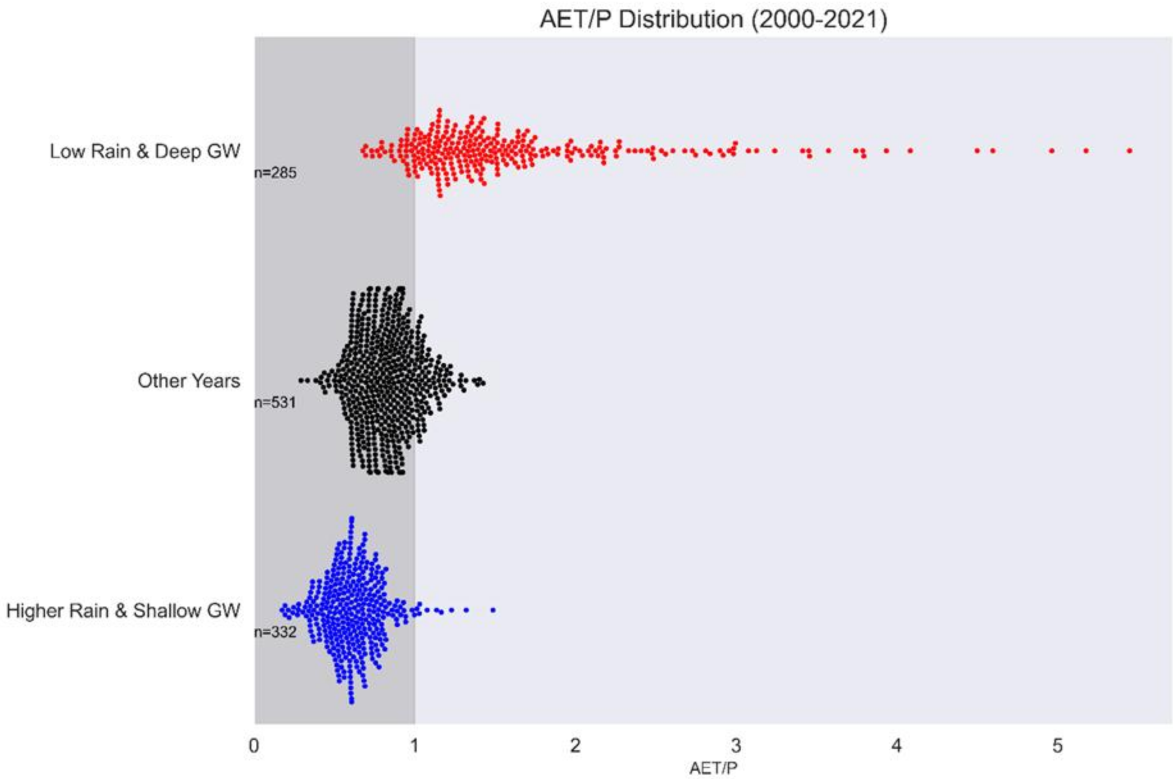

AET/P Distribution (2000-2021)
Low Rain & Deep GW
n=285
Other Years
n=531
Higher Rain & Shallow GW
n=332
0
1
2
3
4
5
AET/P

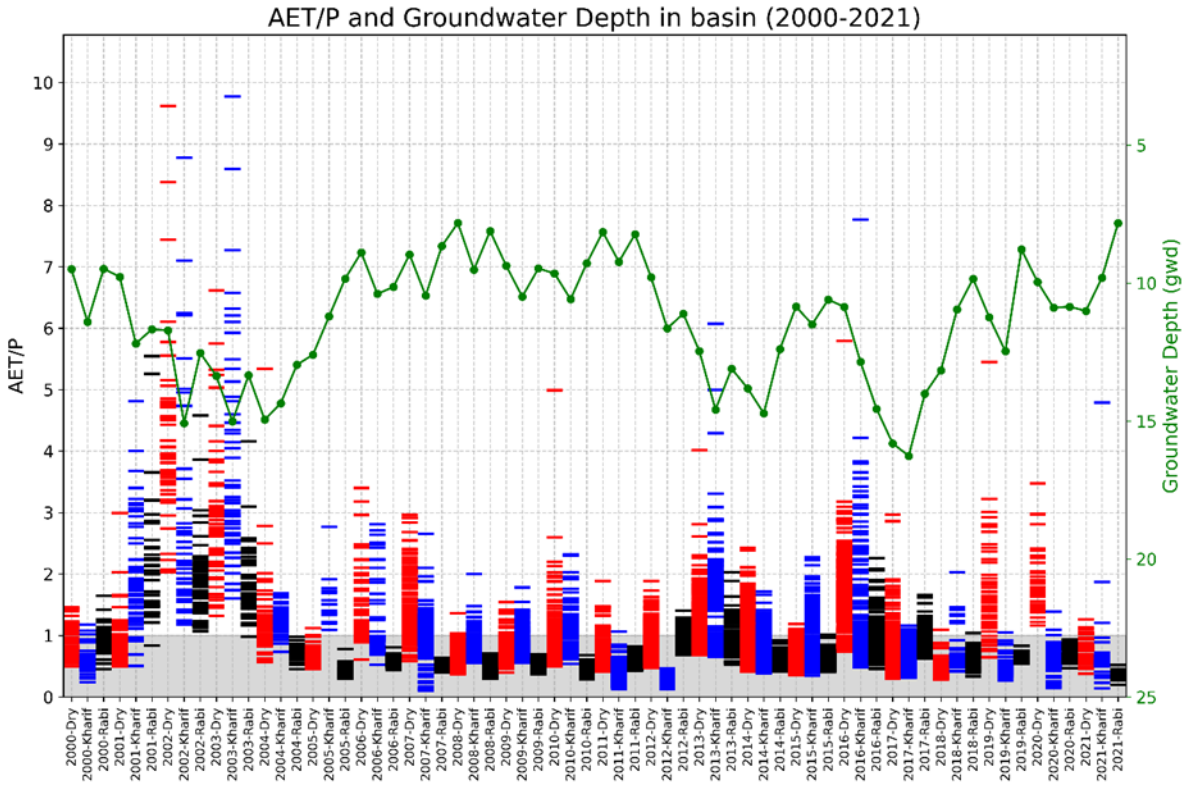
AET/P and Groundwater Depth in basin (2000-2021)
AET/P
Groundwater Depth (gwd)

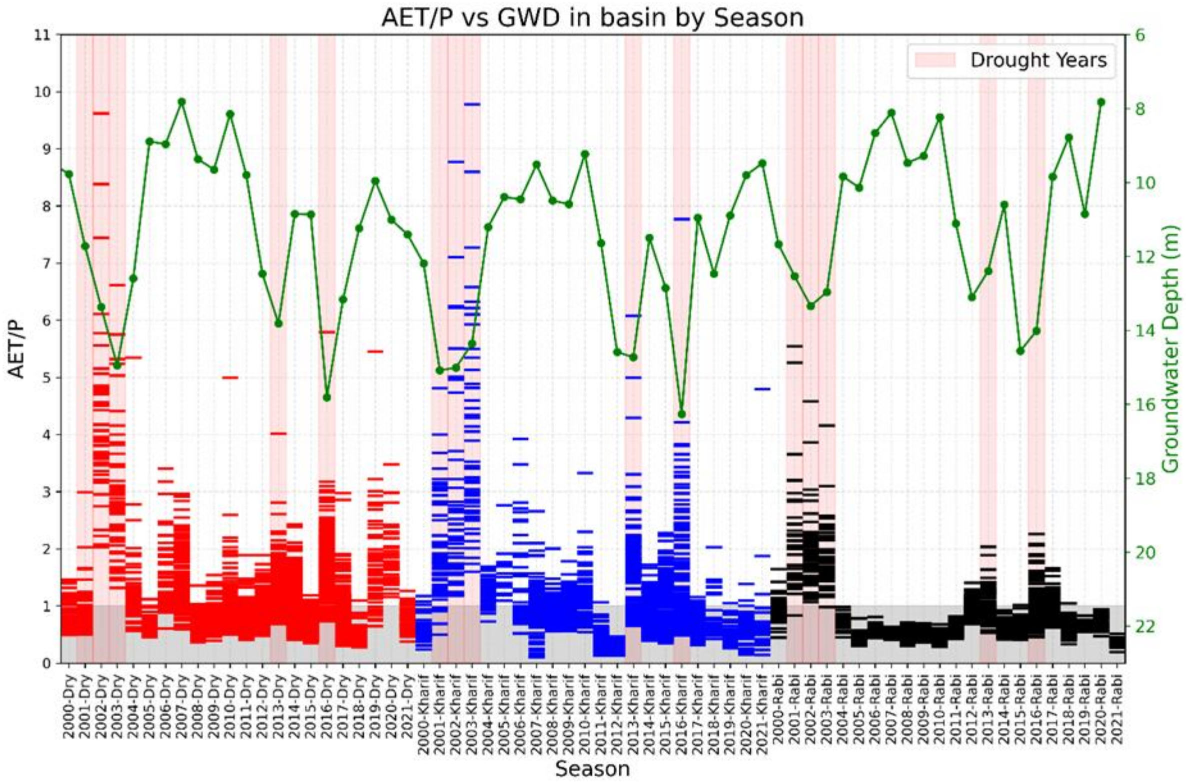
AET/P vs GWD in basin by Season
Drought Years
AET/P
Groundwater Depth (m)
Season